Materials and Structures (2023) 56:123
https://doi.org/10.1617/s11527-023-02210-z

ORIGINAL ARTICLE

# Dynamic enhancing effect of free water on the dynamic tensile properties of mortar

**Xihong Zhang · Yu-Wen Chiu · Hong Hao · Jian Cui**

Received: 30 October 2022 / Accepted: 12 July 2023 / Published online: 27 July 2023


**Abstract** This study investigates free water effect on the dynamic tensile properties of mortar. Fully saturated and saturated-then-redried mortar specimens with two porosities, namely common and high-porosity, are prepared and tested under quasi-static and dynamic split-tension states covering strain rates between 1.49e−06$s^{-1}$ and 5.29$s^{-1}$. The split-tensile strength and elastic modulus at different strain rates are quantified. Comparing the dynamic increase factor (DIF) for mortar tensile strength, a maximum difference of 1.2 at strain rate 5 $s^{-1}$ is found between saturated and dried high-porosity mortars revealing the influence of free water. The testing data is compared with other existing data which shows the mortar water effect is more similar to concrete than limestone and sandstone. The high-speed camera images during the dynamic tests are analysed which revealed a water retarding effect on the dynamic split-tension failure process, resulting in an initial crack delay of up to 0.4 ms due to free water. The wave speed for different mortar specimens at different strain rates is analysed, which shows that higher porosity is more sensitive to the water effect. Possible mechanisms leading to this water effect is discussed. Overall, the study provides a quantitative measure of the water enhancing effect on the dynamic tensile strength of mortar and offers insights into the practical use of water in the design and construction of mortar structures.

**Keywords** Free water · Saturation effect · Hydric deterioration · Split tension · SHPB · Porosity

X. Zhang (✉) · Y.-W. Chiu · H. Hao
Centre for Infrastructural Monitoring and Protection, School of Civil and Mechanical Engineering, Curtin University, Bentley, WA, Australia
e-mail: xihong.zhang@curtin.edu.au

H. Hao
Earthquake Engineering Research and Test Centre, Guangzhou University, Guangzhou, China

J. Cui
Tianjin University, Tianjin, China

## 1 Introduction

Concrete and mortar are porous materials comprising of small and large pores as well as micro-cracks. When submerged in water, these pores and cracks will be filled with water which therefore changes the mechanical properties of concrete and mortar. In the meanwhile, it is known that materials would behave differently under quasi-static and dynamic loading conditions [1–6]. During the service life of a structure such as a dam, bridge pier, etc. it would be in an underwater environment could experience dynamic loading conditions like an earthquake, vehicle or ship impact, falling rock, and deliberate or accidental

explosion loading; therefore, it is important and valuable to quantify the influence of free water on the dynamic material properties of these materials.

There are a few studies that have investigated the concrete and mortar material properties under saturated and dry states [7–12], but the conclusions were radically different due to different concretes with different strengths and porosities, etc., were used in the studies. For instance, some researchers reported the reduced compressive material strength in saturated concrete at quasi-static states, which indicates softening effect induced by free water. But an equivalent or even higher strength was reported on saturated concrete specimens at a high strain rate, indicating the more pronounced strain rate effect on the saturated concrete [10, 13–16]. This phenomenon is attributed to meniscus cracking under the influence of free water. For brittle materials, when they are subjected to dynamic loading the stress wave will propagate through specimens quickly leaving not be sufficient time for cracks to initiate and develop at weaker sections of the specimen. Hard core material crushing resulting in the increased strength of the material. Thus, most brittle materials are sensitive to strain-rate effect irrespective to dry or saturated status [17–20]. Therefore, it is difficult to distinguish whether the observed enhancement is contributed by loading rate or by free water enhancement. On the contrary, Yan and Lin [8] tested dry and saturated concretes using a servo-hydraulic testing system and found a 41% decrease in tensile strength at strain rate $10^{-6}$ $s^{-1}$ and a 22% decrease at strain rate of $1 \times 10^{-0.3}$ $s^{-1}$ on saturated concrete specimens. Wu et al. [18] tested flexural strength of saturated concrete at strain rates in the range of $10^{-6}$ $s^{-1}$and $10^{-3}$ $s^{-1}$, where a reduced strength was also found. Similarly, Petrov et al. [19] and Huang et al. [21] and Huang et al. [22] tested limestone and sandstone, respectively, and also found apparent tensile strength reductions on their saturated samples under quasi-static states, but the reduction declined as the strain rate increased. Recently, Zhou et al. [23] showed that both dry and saturated sandstone were rate sensitive, and an almost constant fracture toughness reduction on saturated sandstones was found. There is no consensus about enhancing or weakening effects of water on material strength which are coupled with the strain rate effect on the dynamic material properties of concrete and mortar.

There are several explanations for the mechanism of free water acting on porous materials, which can be summarised as follows:

(a) Water enhancement effect due to confinement. When loaded, the water pore pressure will increase resulting in extra strength in the saturated specimen than that compacted with air. Previous study by Jin et al. [15] supported this assumption. A three-phase sphere model was proposed which demonstrated that water within pores could limit the deformation of solid matrix nearby leading to a higher Poisson's ratio and Young's modulus of saturated concrete specimens in comparison to dry ones. Similarly, a recent numerical study [24] also proven that the wet concrete stiffness is improved due to the free water inside the pores limits the deformation of the surrounding mortar matrix. Previous study on saturated sandstone [22] also found a higher dynamic tensile strength which was attributed to the confinement by water pore pressure. Nevertheless, it is clear whether this strength increase is due to dynamic material property or water enhancement effect as the strain rate effect also increase the material strength.

(b) Water enhancement effect because of surface tension or adhesive force and the attraction force between solid particles. In the nano-scale, the amount of water and silicon exhibit adhesive force [25, 26]. The contact surface between particles showed that pulling-off force would increase with the rise of relative humidity [27, 28]. The adhesion is dependent on the size of contact and surface roughness, i.e., smaller hydrophilic contacts show a more pronounced increase in adhesion than large hydrophilic contacts.

(c) Water enhancement effect attributed to viscosity effect or Stefan effect. Viscous force could be produced by water interaction with thin layers of the concrete. Rossi [13] depicts Stefan effect analytically as $F = \frac{2Vr\cos\theta}{h^2} + \frac{3nV^2}{2\pi h^2} \times \frac{dh}{dt}$. When the two surfaces slides at a velocity ($V$), an opposing force ($F$) will be produced on the surfaces of an existing crack with a gap ($h$). Recently, Gu et al. [29] found that both material porosity and water content could influence the

liquid film strengthening effect. More apparent cohesive force is observed when the distance of the particle is smaller, which means for a material with higher porosity, less water enhancement effect could be expected. And the adhesive force between particles will increase with the rise of water content until an optimal liquid bridge volume is reached, after which the force will gradually reduce.

(d) Water softening effect due to bursting of pore water to reduce the strength of a material. Water within the gel pore will be loaded when a saturated porous specimen is loaded. It will impose an internal hydro pressure on the surrounding skeleton structure, which would result in crack splitting tensile force, and further reduces the strength of a material [30]. Recent laboratory testing data [31–34] showed that the free water in the pore led to the compressive strength of saturated concrete weakening. Free water particles within voids and cracks could alter the loading path of the solid skeleton, which produces crack splitting force; and the strength degradation would be more significant as material porosity rises [31]. A recent study [33] investigated the compressive strength of the water-saturated concrete, and concrete with recycled with low to high water absorption, respectively. The results showed that the compressive strength of water-saturated concrete is lower than dry concrete. The compressive strength further decreases with the increase of concrete porosity. Also, the fatigue life of saturated concrete is significantly reduced and the compressive fatigue failure mode shifted from splitting failure in dry concrete to combined splitting and shearing failure in saturated concrete and shear failure in water submerged concrete [34]. Since there is not sufficient time for water to flow out of a specimen when it is subjected to dynamic loading. The bursting effect could be more substantial. However, the bursting effect cannot be measured at the macro-level; therefore, no solid evidence can support this theory.

(e) Water softening effect due to hydric expansion. Expandable materials such as clay in concrete and mortar, despite very small quantity, would expand when absorbing free water. It thus leads to micro-cracking in concrete and mortar specimens and deteriorates material mechanical properties. A recent study [35] was performed on the cracking mechanisms of concrete structures in the saturated and unsaturated zones of the foundation using microscopy technologies. It was found that concrete cracking was related to the combined effect of freeze–thaw deterioration and Alkali-Silica Reaction (ASR) of shale particles. A recent study by the authors on dynamic compressive properties of dry and saturated mortars provided evidence to support this hydric expansion induced softening effect.

Most of the above explanations are primarily based on theoretical assumptions and lack direct supporting evidence. The above mechanisms could occur individually or be effective simultaneously which depends on the loading rate, moisture content and the material tested. Therefore, the static and dynamic free water effect on the material is still not fully understood.

Although, the field of concrete deterioration and improvements has seen several advances, such as innovative materials [36], advanced detecting technologies [37], repairing methods [38, 39] and retrofitting techniques [40] to enhance the durability and resilience to reduce the environmental impact on concrete. Among all, the recent advanced studies on micro-nano filler have proven to be a new effetely method to improved material pore structure [41]. Studies such as nanoparticles, nanofibers, nanotubes, and nanosheets, can improve the mechanical performance, wear resistance, and durability of cementitious composites [42]. For example, A study [43] use of pozzolanic nanofillers has been found to significantly enhance the fatigue performance of reactive powder concrete (RPC) by reducing initial defects, inducing compact hardened concrete matrix, and modifying the interfacial transition zone (ITZ) through the nanocore effect. In the study of Geopolymer concrete [44], nano-titania has been found to improve compressive, flexural, and splitting tensile strength. The benefits such as homogenization and densification of the matrix and reduces fluid permeability have been mathematically quantified from studies [45, 46] Overall, Nanofillers can increase material compactness, and enhance the internal space of cement particles as an effective binder material.

To address mortar deterioration issues more efficiently, This study quantified the softening effect of free water on the tensile properties of mortar by comparing the tensile strength of fully dry and saturated-then-redried mortar specimens without any additives. This paper focuses on discovering the potential enhancing effect of free water on the dynamic tensile properties of mortar. Fully saturated and re-dried mortar specimens are prepared to eliminate the influence of hydric expansion induced material deterioration. Then, quasi-static and dynamic tensile tests are conducted to quantify the split-tensile strength and elastic modulus of mortars under different strain rates. The influence of free water in mortar tensile properties is investigated and quantified. The deterioration and improvement will be further investigated in the future studies.

## 2 Laboratory testing setup

### 2.1 Specimen preparation

This study aims to investigate the effects of mortar porosity on the mechanical properties of cement mortar. To achieve this goal, two types of mortar are casted with different mix proportions, resulting in different levels of porosity and strength. The common mortar is casted with a lower water-to-cement ratio and a higher cement content, resulting in a denser structure with a lower porosity and a higher strength. On the other hand, the high-porosity mortar is casted with a higher water-to-cement ratio and lower cement content, resulting in a more porous structure with a lower strength. Portland cement (3150 kg/m$^3$), hydrated lime (2200 kg/m$^3$), sand (1610 kg/m$^3$) and water are mixed with ratios as shown in Table 1. The specimens are mixed and cast in 100 mm diameter by 100 mm length cylinders, which are then cured in the curing room for 28 days, following by cutting and grinding to ensure the surface smooth and parallel and then treated in two groups for each type of mortar. For the group of fully saturated specimens, they are soaked in water tank for 365 days, and the weight of each specimen is monitored until it is stabilised so as to achieve the fully saturated (S) states. Half of these specimens are taken out of water and re-dried in oven as shown in e, to prepare the other group of saturated-then-redried specimens (S-D). Table 1 shows the densities, moisture content and hydric expansion for common mortar and high-porosity mortar.

### 2.2 Split-tensile tests

#### *2.2.1 Quasi-static test*

The split tensile test, also known as the Brazilian test, is a standard testing method used to determine the tensile strength of concrete and other construction materials. In this study, quasi-static split tensile tests are conducted on a universal testing system—Shimadzu-300 with reference to ASTM-D3967 [47]. The loading speed is controlled which resulted in a loading rate of around $1 \times 10^{-5}$ GPa/s to $1 \times 10^{-2}$GPa/s on

**Table 1** Mortar specifications and properties

| | Water/cement ratio | Mixing ratio (cement: lime: sand) | Specific gravity (cement: lime: sand) | Density (dry) kg/m$^3$ | Density (saturated) kg/m$^3$ | Density (saturated to dry) kg/m$^3$ | Moisture content[a] (saturated) | Hydric expansion[b] mm/m |
|---|---|---|---|---|---|---|---|---|
| Common mortar | 0.5 | 1:1:6 | 3.15:2.2:1.61 | 1716 | 1933 | 1674 | 11.2% | 0.14 |
| High-porosity mortar | 0.8 | 1:1:8 | 3.15:2.2:1.61 | 1902 | 2277 | 1817 | 16.5% | 0.39 |

[a] The moisture content is calculated as $w = 1\text{-} \frac{\rho_{dry}}{\rho_{sat}}$, where $\rho_{dry}$ is the density of dry mortar sample and $\rho_{sat}$ is the density of the saturated sample

[b]The hydric expansion is calculated as $\Delta L = 1\text{-} \frac{L_{dry}}{L_{sat}}$, where $L_{dry}$ is the length of dry mortar sample before water immersion and $L_{sat}$ is the length of the saturated sample after the 365-day water immersion

the specimens. Three specimens for each group of mortar are tested at these two loading rates. The specimen is placed between two platens of a testing machine, with a loading cradle to distribute the load evenly over the specimen and to prevent premature concrete crushing damage. A compressive axial load is applied to the specimen using the testing machine, which causes the specimen to break in tension along the centre. The strain rate $\dot{\varepsilon}$ is calculated from the loading rate $\Delta\sigma_t$ over the static elastic modulus $E$ as shown in Eq. (1).

$$\dot{\varepsilon} = \frac{\Delta\sigma_t}{E} \tag{1}$$

where $t$ is the time variation of the increasing stress region.

And the tensile strength $\sigma_T$ is calculated using Eq. (2) as

$$\sigma_T = \frac{2T}{\pi D_s L_s} \tag{2}$$

where $T$ is the applied load, $D_s$ is diameter and $L_s$ is length of the specimen.

### 2.2.2 Dynamic test

The dynamic split-tensile tests are performed using the split-Hopkinson Pressure Bar testing system at the Structural Dynamics Laboratory, Curtin University. SHPB is a testing method used to investigate the dynamic behaviour of materials under high strain rates. The SHPB system used in this study consists of a 0.5 m long striker bar and two long bars, 5 m long indicant bar (100 mm diameter) for the input of the stress pulse and a 3 m long transmitter bar for the output signal; a specimen that is placed in between incident and transmitted bars for dynamic testing parameter illustrations. The bars are made of high-strength tool steel, whose density is 7800 kg/m$^3$ and Young's modulus is 200 GPa. A pair of strain gauges are glued on the surface of the incident and transmitter bars at mid-length to record stress waves. The striker bar impacts the incident bar, generating a compressive stress wave that propagates through the incident bar and into the specimen then transmitted bar. The incident and transmitted bars will deform under the stress wave, which firstly generated with striker to incident bar propagate through the specimen then to transmitted bar; all the signals were measured by the strain gauges.

The SHPB is a high-strain-rate testing apparatus that was originally developed in the early 1940s by Bertram Hopkinson then later modified by Davies [48, 49]. The fundamental assumptions for a split-Hopkinson Pressure Bar test are: 1) the steel bars are in elastic state during the test; 2) there is no premature failure of the tested specimen before stress equilibrium is reached; c) there is minimized end friction. The stresses at the interfaces between specimen and the incident bar ($\sigma_1$)/transmitter bar ($\sigma_2$) are defined and checked for equilibrium

$$\sigma_1 = E_b(\varepsilon_{\text{ref.}} + \varepsilon_{\text{inc.}}) \tag{3}$$

$$\sigma_2 = E_b\varepsilon_{\text{tra.}} \tag{4}$$

where $E_b$ is the Young's modulus of the bar; $\varepsilon_{ref.}$, $\varepsilon_{tra.}$ and $\varepsilon_{inc.}$ are the reflected, transmitted and incident strains measured on the incident and transmitted bars by strain gauges.

The strain rate that the specimen experienced ($\dot{\varepsilon}$) can be calculated using Eq. (5)

$$\dot{\varepsilon} = \frac{C_b}{L_s}(\varepsilon_{ref.} + \varepsilon_{tra.} - \varepsilon_{inc.}) \tag{5}$$

where $C_b$ is the wave speed, $L_s$ is specimen length.

The stress and strain of the specimen can be expressed as

$$\sigma_s = \frac{E_b A_b}{A_s}\varepsilon_{tra.} \tag{6}$$

$$\varepsilon_s = \frac{2C_b}{L_b}\int_{ref}^{\varepsilon} dt \tag{7}$$

where $\sigma_s$ is the transmitted stress from the transmitter bar, $A_b$ and $A_s$ are the cross-section area of the bars and the test specimen, respectively, $\varepsilon_s$ is the strain of the specimen, $L_{b.}$ is the length of the bar.

Figure 1 illustrate a typical group of stress wave from the incident bar and the transmitter bar. For a valid test, it should also be able to satisfy the following conditions: (1) dynamic stress equilibrium is achieved in the test specimen. The fundamental differences between dynamic test and static test is that the inertia effect are wave propagation are pronounced especially when the specimen is experiencing high strain rates. It is crucial for the stress and strain within the tested specimen being uniform; and (2) stress impedance

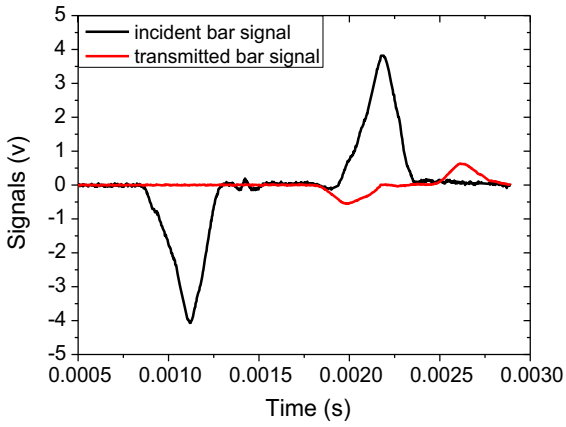


**Fig. 1** Typical stress wave signals

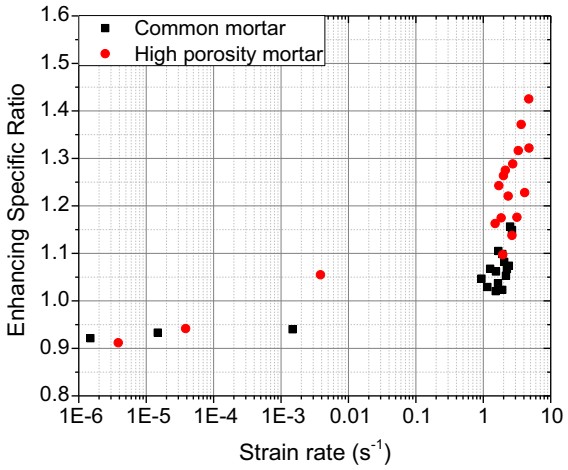


**Fig. 2** specific enhancing ratio

between the tested specimen and incident/transmitter bars should be minimized. Dynamic equilibrium is carefully checked to ensure the validity of each high-speed compressive test.

## 3 Results and discussions

### 3.1 Test results

The quasi-static test results are shown in Appendix A. For the common mortar, the saturated specimens have an averaged quasi-static ($\dot{\varepsilon} = 1.49 \times 10^{-6}$ s$^{-1}$) split-tensile strength of 1.09 MPa, while that for the dry specimen is 1.19 MPa, indicating a slightly higher strength for dry mortar. As strain rate increases to $1.49 \times 10^{-5}$ s$^{-1}$, the averaged split-tensile strength is 1.15 MPa for the saturated mortar specimens in comparison to 1.23 MPa for the dry specimens with a difference of 7.3%. At a strain rate of $1.49 \times 10^{-3}$ s$^{-1}$, the saturated specimens have an averaged split tensile strength of 1.25 MPa, and that for the dry mortar is 1.33 MPa, i.e.,6.4% higher than the saturated ones. Similarly, for the high-porosity saturated mortar, the averaged split-tensile strengths are 0.32 MPa, 0.35 MPa and 0.45 MPa at strain rates of $3.85 \times 10^{-6}$ s$^{-1}$, $3.85 \times 10^{-5}$ s$^{-1}$, and $3.85 \times 10^{-3}$ s$^{-1}$, in comparison to 0.35 MPa, 0.37 MPa and 0.43 MPa for the corresponding dry specimens. These results demonstrate that at quasi-static and low strain rate, free water in mortar leads to slight reductions in the split-tensile strength of mortar, but the influence of free water on reducing the split tensile strength as compared to that of dry mortar monotonically decreases as strain rate increases. The influences of free water on the split tensile strength of common mortar and high-porosity mortar have similar trend, although the split tensile strength of high-porosity mortar is substantially lower than the common mortar.

The dynamic testing results are shown in Appendix B. Both strain rate and loading rate are used to describe dynamic testing results in this study. The loading rate is calculated by differentiating the stress over time. The linear increment gradient of the stress strain curve for each specimen from the dynamic test is employed as the elastic modulus $E$. The strain rate covers a range from 0.94 s$^{-1}$ to 2.94 s$^{-1}$ for common mortar and 1.5 s$^{-1}$ to 5.29 s$^{-1}$ for the high-porosity mortars. For the common mortar, the split-tensile strength of the saturated specimens increases from about 1.32 MPa to 2.25 MPa, while that of the dry specimens increases from about 1.45 to 2.20 MPa, both showing an increasing trend with strain rates. The strength of saturated specimens appears to be slightly higher than those of the dry specimens at similar strain rates, indicating enhancing effect. Similarly, for the high-porosity mortar, the split-tensile strength of saturated specimens ranges from 0.53 to 1.07 MPa, which shows higher strength than those of the re-dried specimens, i.e. DB-CM-SD (from 0.45 to 0.90 MPa). In Fig. 2, The enhancing specific ratio show that the existence of free water enhances the dynamic split-tensile strength of mortar as strain rate increases. The enhancement is more significant when porosity is higher because of the

high water content. These results indicate the saturated specimen is more sensitive to strain rate effect than the dry specimen and the strain rate sensitivity increases with the water content of the specimen.

### 3.2 Stress–strain curves

Figures 3 and 4 show the stress–strain curves at different strain rates. As depicted, the split tensile strengths of both saturated and dry mortars (including common and high-porosity mortars) are all strain rate sensitive. The split-tensile strength increases with strain rate, and the corresponding elastic modulus also shows a slight increase with strain rate. It is worth noting that the stresses of the saturated mortars show a smooth linear increasing trend with larger plastic or post-peak strains than the dry (SD) mortars, indicating the saturated mortars have better plastic deformation capacity. A previous study by Hashiba and Fukui [50] on dry and wet rock found similar results that the crack extension resistant force of wet rock was slightly greater than the dry rock at the same stress.

### 3.3 Dynamic fracturing process

Figure 5 shows the dynamic fracturing process of typical mortar specimens at similar strain rates during the dynamic tests. A high-speed camera captures the images with a filming rate of 0.4 ms per image. For the dry (SD) common mortar specimen, as shown in Fig. 6a), a crack is initiated from the centre of the specimen at $t$ = 0.4ms, which extends laterally towards the two ends of the specimen. At $t$ = 0.8ms, the central crack grows wider, and multiple cracks are developed at the edge at $t$ = 1.2 ms leading to the eventual failure of the specimen. This observation proves the validity of the dynamic split tension test. In comparison, for the saturated (S) common mortar specimen (Fig. 6b), a crack initiates at about $t$ = 0.8ms from the centre of the specimen, which occurs later than the dry specimen as shown in Fig. 4a). This crack quickly extends towards both ends of the specimen leading to the eventual failure. This comparison demonstrates that free water inside the mortar could postpone the cracking instance within mortar specimens. Similar observation can be found on the high-porosity mortar specimens, as shown in Fig. 6c and d. It is worth noting that due to equipment constraints, the exact crack initiation instant could not be captured, but it is evident that free water apparently delays the crack initiation in the saturated mortar specimens for 0–0.4ms.

Significant differences can be overserved from comparing both static and dynamic fracturing failure. 1. The stress concentration is more server on much higher loading rate impact. The fast loading stress waves much more easier to develop a stress concentration near the sample edge area from the impact side, leading a different stress distribution. similarly, studies found inertia effect is more dominant during dynamic impacts. 2. Material strain rate sensitivity is found higher on high-porosity mortar as multiple cracks are easier to be observed from dynamic failure of HP mortar than common mortar. 3. Sample fragment are radically

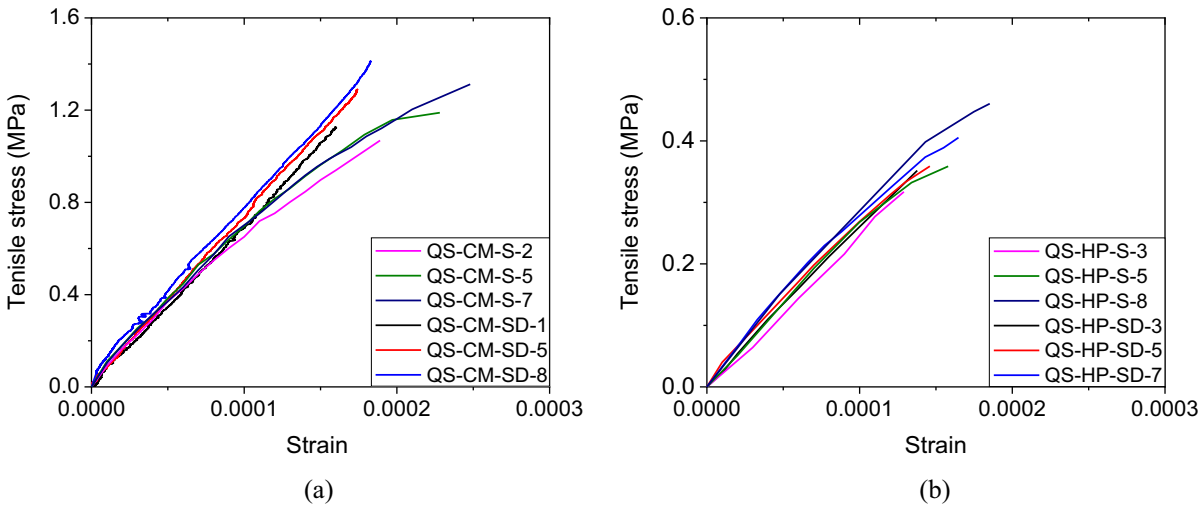


**Fig. 3** Quasi-static stress–strain curves: **a** CM; **b** HP

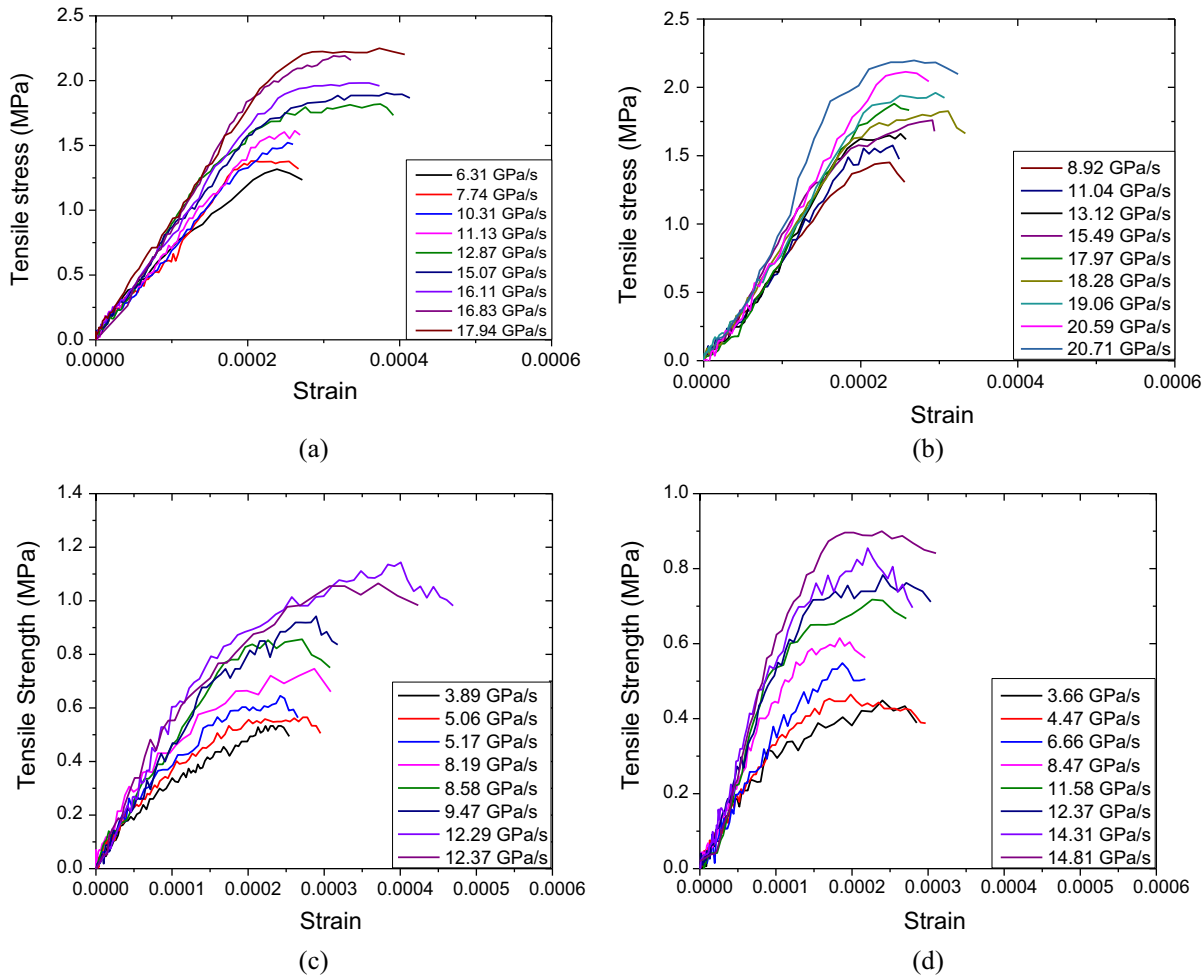


**Fig. 4** Dynamic stress–strain curves: **a** CM-S; **b** CM-SD; **c** HP-S; **d** HP-SD

different for static and dynamic failure samples Higher number of smaller fragment pieces and finer powder were produced from dynamic test from multiple crack failure instead only two whole broken pieces from static test, such effect is more significant on HP sample as well. 4. Energy absorption is higher on dynamic samples due to multiple cracks were formed and more fragment were broken into pieces which require higher stress to create multiples failure path.

## 4 Analysis and discussion

### 4.1 Water retarding effect

High-speed camera images in Sect. 3.3 show that crack initiation is delayed in saturated mortar specimens. To further examine the observation, transmitted stress waves recorded on the transmitter bar of the SHPB system for the saturated (S) and dry (SD) mortar specimens subjected to the same striker bar velocity are compared in Fig. 6. It can be observed that the recorded stress wave is affected by the saturation states of the specimens. The saturated specimen has a lower increasing gradient as well as a lower peak stress indicating the water is slowing down the stress wave transmission and the deformation of the specimen, which results in a lower material strength and a lower loading rate (14.7 GPa/s). In comparison, the dry (SD) mortar specimen experienced a higher loading rate (10.3 GPa/s) during the dynamic split-tensile test, as indicated in the figure. The above comparison demonstrates the influence of

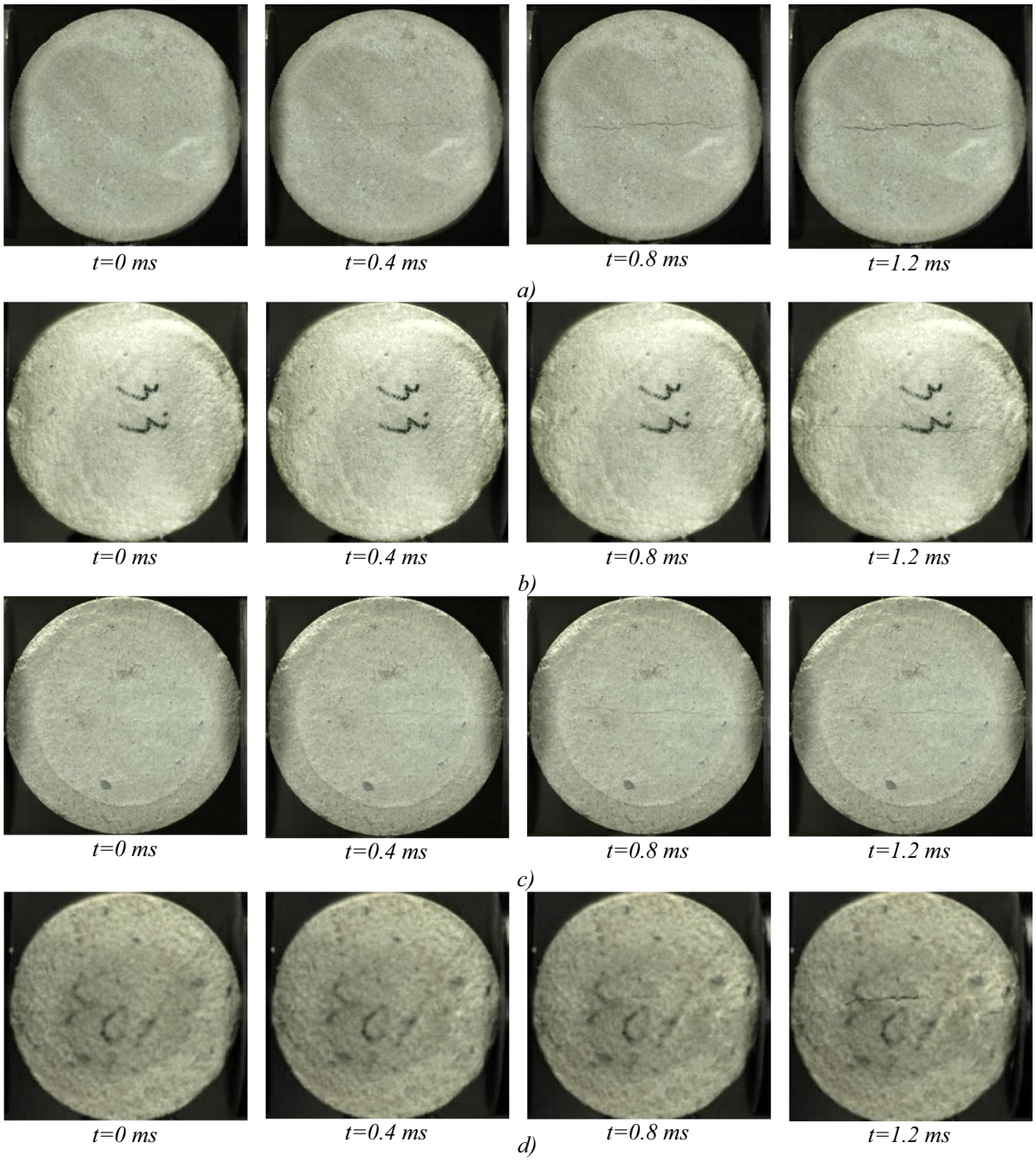


**Fig. 5** Dynamic fracturing processes: **a** CM-SD; **b** CM-S; **c** HP-SD; **d** HP-S

free water in the mortar specimen would retard stress wave propagation in mortar.

The P-wave velocity, $C_e$, which can be calculated by Eq. (8), is employed in the analysis to examine the water retarding effect.

$$C_e = \sqrt{\frac{E}{\rho}} \tag{8}$$

where $E$ is the dynamic modulus of the specimen and $\rho$ is the specimen material density.

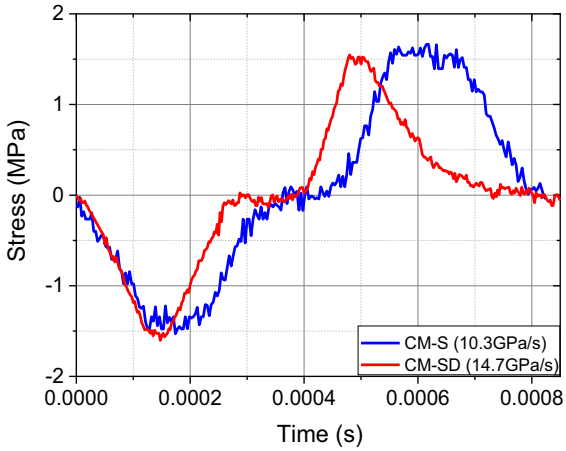


**Fig. 6** Comparison of transmitted stress waves between saturated (S) and dry (SD) mortar specimens

As shown in Fig. 7, the P-wave velocity of the saturated common mortar obtained based on the measured modulus and density of the specimens presented above is apparently smaller than that of the dry (SD) specimen. Similarly, for the high-porosity mortar, the wave velocities of the saturated specimens are also noticeably lower than those of the dry (SD) specimens. It is apparent that free water in mortar could slow down the wave speed in the mortar specimens. It can also be noted that the wave velocity of the high-porosity mortar is much lower than those of the common mortar; this is because of the smaller modulus of the high-porosity mortar due to more voids.

## 4.2 Strain rate effect

Testing results in Sect. 3 show the strain rate effect on the split-tensile strength and modulus of mortar. Figure 8a and b plot the tensile strengths versus loading rate. It can be found that the tensile strengths of the tested mortar show apparent rate sensitivity, which all increase as the loading rate increases. For the common mortar, the dynamic tensile strength of the dry (SD) mortar is 1.45 MPa at a loading rate of 8.92 GPa/s. As the loading rate increases, the strength rises to 2.20 MPa at a loading rate of 20.71 GPa/s. The saturated mortar has a slightly lower tensile strength of 1.32 MPa at a loading rate of 6.31 GPa/s, which increases to 2.25 MPa at a loading rate of 17.94 GPa/s. The saturated specimens have slightly higher tensile strength than the dry (SD) specimens at a similar loading rate. And the difference becomes more apparent as the loading rate increases. This phenomenon is more prominent in the high-porosity mortar that a very significant enhancement effect can be observed on the saturated mortar as compared to the dry (SD) specimens. The comparison demonstrates that free water in mortar could provide an enhancement effect on the tensile strength of mortar, which becomes more significant as the loading rate increases. This is probably because of water viscosity. The existence of free water in the cracks and voids within the mortar specimens provides a viscous force that is related to the loading rate. It is found that the water enhancement effect on mortar tensile strength

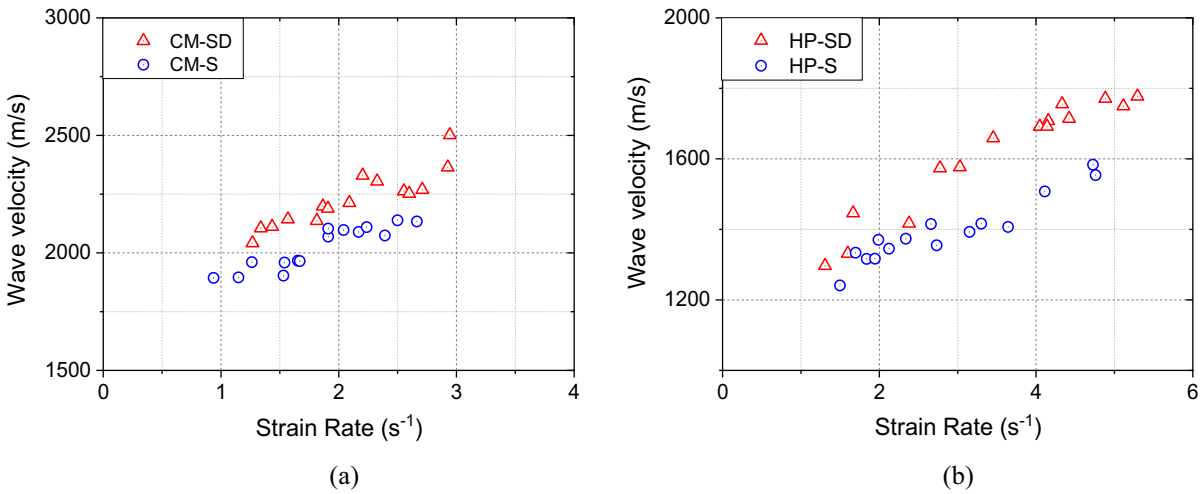


**Fig. 7** P-wave velocity vs. strain rate a) common mortar; b) high-porosity mortar

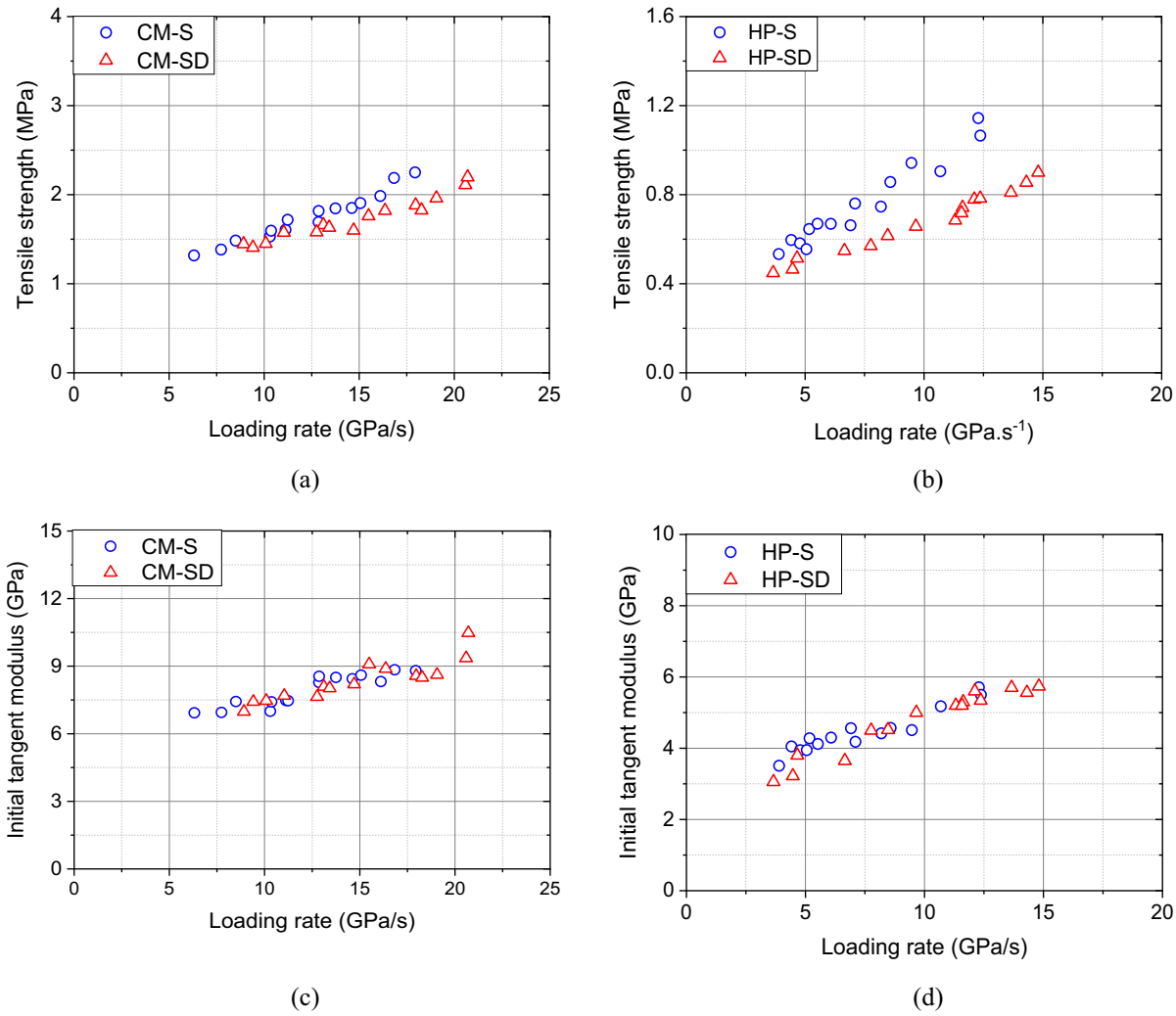


**Fig. 8** **a** dynamic strength vs. loading rate for CM; **b** dynamic strength vs. loading rate for HP; **c** dynamic modulus vs. loading rate for CM; **d** dynamic modulus vs. loading rate for HP

increases with the mortar porosity. This is because, with more sand and less cement in the high-porosity mortar, there are more cracks and voids. When submerged in the water, there is more water in the saturated specimens; hence water enhancement effect becomes more significant. Similarly, the modulus (Fig. 8c and d) also appears to be loading rate sensitive. For the saturated common mortar, an average modulus of 7.03 GPa is measured under a quasi-static loading condition, which increases to 7.0 GPa at 8.92 GPa/s and further increases to 9.4 GPa at a loading rate of 20.59 GPa/s. A similar trend can be found on the dry (SD) common mortar specimens, which nevertheless show the strain effect on the modulus, instead of the water effect. A similar finding can be found on the high-porosity mortar that the modulus is sensitive to loading rate, which nevertheless is not related to the free water.

### 4.3 Empirical equations of DIF

DIF for mortar tensile strength is derived by dividing the dynamic tensile strength by the averaged quasi-static strength, and DIF for mortar modulus is determined by dividing the dynamic modulus by the averaged modulus measured at quasi-static states.

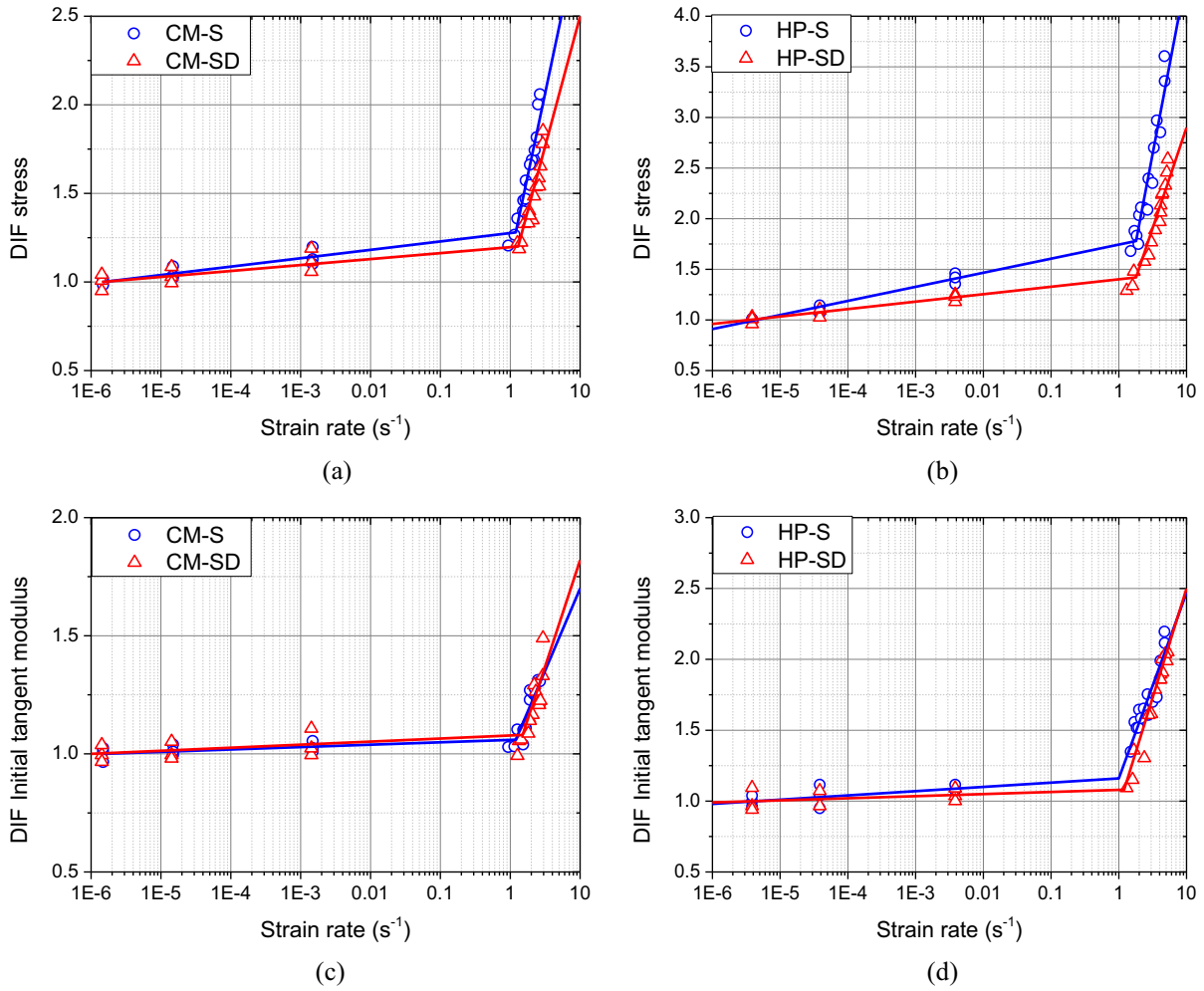


**Fig. 9** DIF vs strain rate relations: **a** tensile strength for CM; **b** tensile strength for HP; **c** modulus for CM; **d** modulus for HP

Through linear regression on the testing data, trend lines are generated as shown in Fig. 9. It can be seen that from a strain rate of 1.5 $s^{-1}$, the DIF of both mortar strength and modulus show strong strain rate sensitivity. Empirical formulae are derived for DIF of tensile strength and modulus as below:

Common mortar

$$DIF_{f,S} = \begin{cases} 0.0475\log(\dot{\varepsilon}) + 1.278 when 10^{-6} \le \dot{\varepsilon} \le 1.2 \\ 1.818\log(\dot{\varepsilon}) + 1.147 when 1.2 \le \dot{\varepsilon} \le 10 \end{cases} \quad (9)$$

$$DIF_{f,SD} = \begin{cases} 0.0403\log(\dot{\varepsilon}) + 1.234 when 10^{-6} \le \dot{\varepsilon} \le 1.3 \\ 1.557\log(\dot{\varepsilon}) + 0.978 when 1.3 \le \dot{\varepsilon} \le 10 \end{cases} \quad (10)$$

$$DIF_{E,S} = \begin{cases} 0.0096\log(\dot{\varepsilon}) + 1.058 when 10^{-6} \le \dot{\varepsilon} \le 1.2 \\ 0.733\log(\dot{\varepsilon}) + 0.997 when 1.2 \le \dot{\varepsilon} \le 10 \end{cases} \quad (11)$$

$$DIF_{E,SD} = \begin{cases} 0.0144\log(\dot{\varepsilon}) + 1.082 when 10^{-6} \le \dot{\varepsilon} \le 1.5 \\ 0.916\log(\dot{\varepsilon}) + 0.903 when 1.5 \le \dot{\varepsilon} \le 10 \end{cases} \quad (12)$$

High-porosity mortar

$$DIF_{f,S} = \begin{cases} 0.139\log(\dot{\varepsilon}) + 1.742 when 10^{-6} \le \dot{\varepsilon} \le 1.8 \\ 3.486\log(\dot{\varepsilon}) + 0.903 when 1.8 \le \dot{\varepsilon} \le 10 \end{cases} \quad (13)$$

$$DIF_{f,SD} = \begin{cases} 0.073\log(\dot{\varepsilon}) + 1.397 when 10^{-6} \le \dot{\varepsilon} \le 1.8 \\ 1.989\log(\dot{\varepsilon}) + 0.922 when 1.8 \le \dot{\varepsilon} \le 10 \end{cases} \quad (14)$$

$$DIF_{E,S} = \begin{cases} 0.030\log(\dot{\varepsilon}) + 1.162 when 10^{-6} \le \dot{\varepsilon} \le 1 \\ 1.313\log(\dot{\varepsilon}) + 1.155 when 1 \le \dot{\varepsilon} \le 10 \end{cases} \quad (15)$$

$$DIF_{E,SD} = \begin{cases} 0.0152\log(\dot{\varepsilon}) + 1.077 when 10^{-6} \le \dot{\varepsilon} \le 1.2 \\ 1.521\log(\dot{\varepsilon}) + 0.942 when 1.2 \le \dot{\varepsilon} \le 10 \end{cases} \quad (16)$$

where $DIF_{f,S}$ and $DIF_{f,SD}$ are the *DIF* of tensile strength for the saturated and dry mortar, $DIF_{E,S}$ and $DIF_{E,SD}$ are the *DIF* of modulus for the saturated and dry mortar, and $\dot{\varepsilon}$ is the strain rate.

### 4.4 Free water enhancing effect

As discussed in the introduction, both strength softening and enhancement effects are observed on saturated and dry concrete and mortar as a result of free water effect. Our previous study also quantified water soaking would lead to hydric expansion which results in strength softening. In the meanwhile, testing data herein demonstrates free water could also provide enhancing effect on saturated mortar specimens, while it appears this enhancing effect is also dependent on the strain rate that the specimen experiences. To quantify the influence of free water to mortar tensile strength, the dynamic strength of a saturated specimen $\sigma_s$ can be expressed as

$$\sigma_S = \sigma_{mat,QS} + \Delta\sigma_{dyn} - \sigma_{w,soft} + \sigma_{w,enhancing} \quad (17)$$

where $\sigma_{mat,QS}$ is the mortar quasi-static strength, and $\Delta\sigma_{dyn}$ is the dynamic strength increment; $\sigma_{w,soft}$ represents the hydric expansion induced softening, and $\sigma_{w,enhancing}$ represent free water induced enhancement.

The strength of a re-dried (SD) specimen $\sigma_{SD}$ can be expressed as

$$\sigma_{SD} = \sigma_{mat,QS} + \Delta\sigma_{dyn} - \sigma_{w,soft} \quad (18)$$

Thus, water enhancing effect can be expressed as

$$\sigma_{w,enhancing} = \sigma_S - \sigma_{SD} \quad (19)$$

A tensile strength enhancing ratio due to free water enhancing effect,$\Delta\sigma_t$, can be introduced as:

Figure 10 shows the calculated strength-enhancing ratio as a result of the water effect. It can be seen that for both the common mortar and high-porosity mortar tested in this study, under quasi-static and low strain rates, the strength increment ratio is negative, indicating strength degradation in the saturated mortar specimens. This is because the existence of free water would act in mortar specimens as a lubricant between particles resulting in a lower localised shear stress resistance [51]. Dudko et al. [52] studied particle bond behaviour on the micro-scale. It was found that the kinetic energy between molecules reduces with the existence of free water; thus, chemical bonding is weakened. Free water in voids and micro-crack weakens the van der waals forces between solid particles. This phenomenon is especially apparent in the rupture force or pulling force when there is sufficient time for the particle to respond, such as under quasi-static loading conditions. Under dynamic loading states, the strength-enhancing ratio becomes a positive value reflecting water enhancing effect. As strain rate/loading rate increases, the strength-enhancing ratio also grows with strain rate and loading rate. This is because the electrical double layers and the reconstruction of water in the contact area between particles, free water in the voids and micro-cracks of mortar specimens could provide substantially more adhesive and viscous forces as compared to air [53]. The water viscous effect becomes dominant, which is highly dependent on loading speed. A higher strength-enhancing ratio can be found on the high-porosity mortar compared to common mortar because of more voids and, therefore, more free water in the saturated specimens. It is also worth noting that a previous study found that free water in saturated mortar specimens would lead to the reduced dynamic compressive strength because there is not sufficient time for water to be squeezed out of the pores. Hence, pore water pressure will be developed at the tip of the crack, thus accelerating the development of inner cracks resulting in strength reduction [30]. However, such excess pore water pressure would not be developed when the specimen is subjected to high-speed tension. Instead, water adhesive force and viscous force become predominant when the specimen is pulled apart under

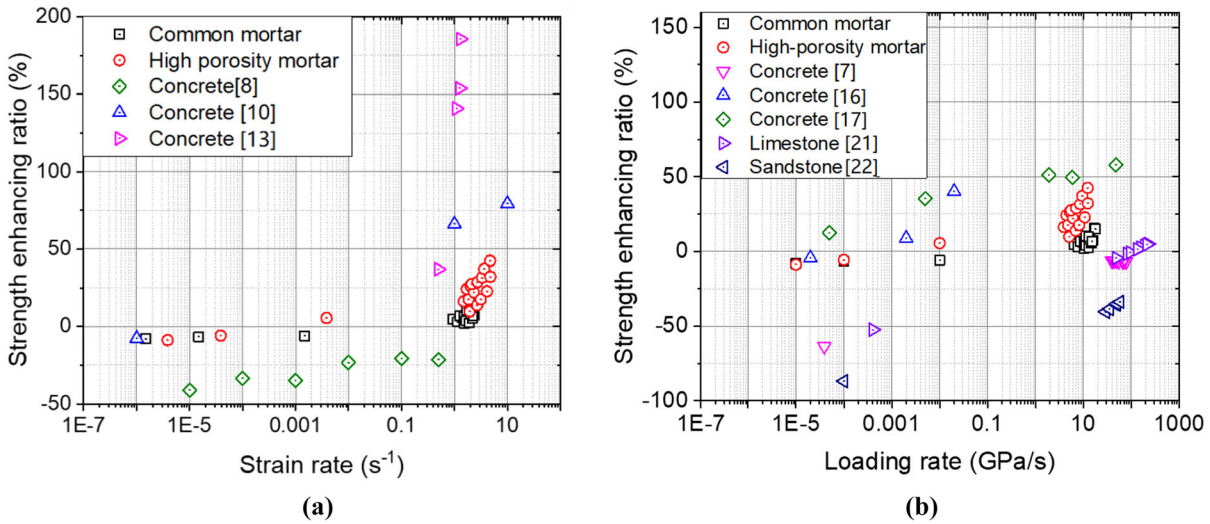


**Fig. 10** Water enhancing ratio vs. **a** strain rate; **b** loading rate

tensile forces, generating the dynamic strength-enhancing effect leading to an increased strength with strain rate/loading rate.

Existing testing data on dry and saturated concrete, sandstone and limestone from different researchers are also included for comparison and analysis. Since some existing data only provide loading rate or strain rate without a modulus, as in Fig. 9, the strength enhancing ratio is thus compared separately versus strain rate and loading rate. Wang et al. [16] tested concrete under dry and saturated states to study the saturation effect on concrete properties. A similar trend was found in this study that a 4.3% strength reduction at a loading rate of $2 \times 10^{-5}$ GPa/sand a strength increment of 40.2% at a loading rate of $2 \times 10^{-2}$ GPa/s on the saturated concrete in comparison to the dry concrete specimens. Similarly, as shown in Fig. 9a, Candoni et al. [10] observed a -7.6% reduction in concrete tensile strength at a strain rate of $10^{-6}$ $s^{-1}$ but a strength enhancement of 79% at a strain rate of 10 $s^{-1}$ on saturated concrete specimens. In the meanwhile, some existing data also show contradicting conclusions. For instance, Yan and Lin [8] studied the water saturation effect on the tensile strength of concrete in the strain rate range of $10^{-5}$ $s^{-1}$ and $10^{-0.3}$ $s^{-1}$. Consistent strength reduction was observed on the saturated concrete specimens, where the strengths of the saturated concrete specimens were found to drop by -41.2% and -21.4% of the corresponding dry concrete specimens. Huang et al. [22] examined the tensile strength of sandstone. The strength of the saturated specimen was found to reduce substantially by nearly -87% as compared to the dry specimen at a loading rate of $1 \times 10^{-4}$ GPa/s. As the loading rate increases, the strength of saturated sandstone increases resulting in an about − 40% lower strength compared to that of dry specimens at about 30GPa/s. Another study by Petrovi et al. [21] on limestone found the tensile strength of saturated limestone is − 52% lower than dry limestone at quasi-static state, but as strain rate increases, an apparent increasing trend can be seen, where the strength of saturated limestone was found to show a 5% increase comparing to the dry limestone specimen at loading rate of about 224 GPa/s since the process of submerging specimens into the water to achieve saturation states could result in material swelling and shrinkage, i.e., hydric expansion, which deteriorates specimen integrity and causes damages. It is difficult to distinguish whether the above weakening effect on material strength is resulted from hydric expansion due to water soaking or purely from free water in the microstructure. Moreover, it is also found that some data, even from the same authors, show substantial saturation effects on material strength. For example, Rossi et al. [7] performed tensile tests on dry and saturated concrete specimens and found the tensile strength of saturated specimen reduced by over -60% under a quasi-static state. The authors attributed the substantial strength reduction to premature edge failure of the dumbbell shape sample during the test,

where an unequally distributed stress caused severe premature failure in the saturated concrete. Nevertheless, it was also found that under dynamic loading condition, the strength reduction ratio dropped to less than 10%, indicating such changes in concrete strength is loading rate sensitive. In a later study also by Rossi et al. [17], tensile strength increment of 13% to 58% from loading rate $5 \times 10^{-5}$ to 50 GPa/s were reported on the concrete, indicating water enhancing effect[13] can rapidly increase the concrete strength from 37 to 186% when strain rate increases from 0.5/s to 1.3 $s^{-1}$.

### 4.5 Empirical formula of water enhancing effect

Empirical formula is derived based on the testing data in this study to predict the strength-enhancing effect of free water. The strength-enhancing ratio $\Delta\sigma_t$ is related to both the strain rate $\dot{\varepsilon}$ and the porosity of material $v$, which thus can be expressed as

$$\Delta\sigma_t = \begin{cases} a\log(\dot{\varepsilon}) + b when 10^{-6} \le \dot{\varepsilon} \le 1 \\ c\dot{\varepsilon} + d when 1 \le \dot{\varepsilon} \le 10 \end{cases} \quad (21)$$

in which

$a = 45\ \mathrm{v} - 3$

$b = 1256\Delta\sigma_{t,s} - 95.85$

$c = 4.5\ \mathrm{v} + 4.7$

$d = 1231\Delta\sigma_{t,s} - 99.09$where $v$ is the porosity; $\Delta\sigma_{t,s}$ is the static reduction ratio (0.088 and 0.079 for CM and HP, respectively).

From Fig. 11 it can be seen that under quasi-static and low-speed tension, free water primarily shows a weakening effect, which appears to be insensitive to strain rate. Under dynamic tension, the strength-enhancing ratio increases quickly with strain rate. Nevertheless, due to the testing condition in this study, the coverage strain rate is limited to about 5 $s^{-1}$. The accuracy of the empirical formula beyond this strain rate range needs future validation.

## 5 Conclusion

This study conducts quasi-static and dynamic split tensile tests on saturated and re-dried mortar specimens to investigate the influence of free water on the tensile properties at different strain rates. Two types of mortars, i.e., common mortar and high porosity mortar, are examined to study the influence of porosity. The testing method developed in this study effectively rules out the influence of water-induced hydric expansion damage to mortar for a more accurate quantification of the free water effect. The following conclusions are drawn from this study:

a) It is found that under quasi-static state, free water in mortar would reduce the split tensile strength resulting in the strength reductions.
b) Under dynamic loading, free water could influence the tensile properties of mortar. The strength enhancement effect is observed where the saturated mortar specimens have a higher dynamic tensile strength than that of dry specimens which up to 42% enhancing ratio on high-porosity mortar.
c) High-speed camera images show that the cracking-to-failure process of saturated mortars is delayed by free water, which shown water retarding effect can up to 0.4 ms. The testing data also confirm that saturated specimens have smaller wave velocities than dry specimens.
d) Both dry and saturated mortars show a strong strain rate effect on tensile strength and elastic modulus. The saturated mortar is more sensitive to strain rate than dry mortar. The relationships of DIF versus strain rate are derived for mortar with a difference up to 1.2 at strain rate 5 $s^{-1}$ between saturated and dried high-porosity mortars.
e) Water enhancing effect is found to be both strain rate sensitive and material porosity dependent with enhancing ratio increase from 0.09 to 0.2 at strain rate 2 $s^{-1}$ for common mortar and high-porosity mortar respectively.
f) Strength enhancing ratio by free water on mortar is quantified. An empirical formula for determining enhancing ratio is derived based on the testing data.

The study reveals that free water has a significant effect on the split-tensile strength of mortar, which increases as the strain rate increases. The enhancing effect of free water on the dynamic tensile strength of mortar is quantified and the possible mechanisms leading to this effect are discussed. The study also compares the test results with existing data from other researchers, which show that free water could cause

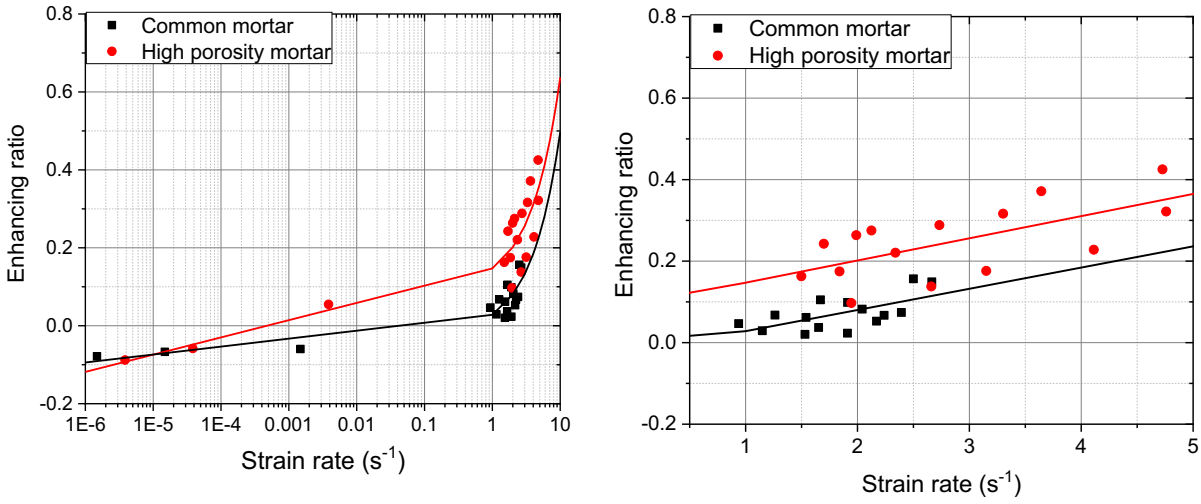


**Fig. 11** Empirical prediction formula of water enhancing ratio to mortar tensile strength

different levels of dynamic tensile strength enhancement. The findings of this study can be used to improve the design and performance of mortar in various engineering applications. particularly in the design of structures that are exposed to dynamic loading, such as bridges, tunnels, and earthquake-resistant buildings. Also, this studying lead to the development of new mortar mix designs and the potential optimization direction to improved performance on porous and cementious materials, which could result in more durable and resilient structures.

**Acknowledgements** The authors would like to acknowledge the financial support from Australian Research Council for carrying out this study.

**Funding** Open Access funding enabled and organized by CAUL and its Member Institutions.

**Declarations**

**Conflict of interest** The authors declare that they have no known competing financial interests or personal relationships that could have appeared to influence the work reported in this paper.



## Appendix A: Quasi-static test results

See Table 2

**Table 2** Quasi-static test results

| Specimen No | $\dot{\varepsilon}$ ($s^{-1}$) | $f_t$ (MPa) | Strain (mm/mm) | $E$ (GPa) |
|---|---|---|---|---|
| QS-CM-S-1 | 1.49E−06 | 1.11 | 0.000193 | 6.8 |
| QS-CM-S-2 | 1.49E−06 | 1.09 | 0.000176 | 6.9 |
| QS-CM-S-3 | 1.49E−06 | 1.07 | 0.000188 | 6.5 |
| QS-CM-S-4 | 1.49E−05 | 1.12 | 0.000219 | 6.7 |
| QS-CM-S-5 | 1.49E−05 | 1.19 | 0.000228 | 7.0 |
| QS-CM-S-6 | 1.49E−05 | 1.13 | 0.000218 | 6.8 |
| QS-CM-S-7 | 1.49E−03 | 1.31 | 0.000232 | 7.1 |
| QS-CM-S-8 | 1.49E−03 | 1.23 | 0.000251 | 6.8 |
| QS-CM-S-9 | 1.49E−03 | 1.20 | 0.000248 | 6.9 |
| QS-CM-SD-1 | 1.42E−06 | 1.13 | 0.000160 | 7.0 |
| QS-CM-SD-2 | 1.42E−06 | 1.20 | 0.000178 | 6.8 |
| QS-CM-SD-3 | 1.42E−06 | 1.24 | 0.000167 | 7.3 |
| QS-CM-SD-4 | 1.42E−05 | 1.22 | 0.000176 | 7.0 |
| QS-CM-SD-5 | 1.42E−05 | 1.29 | 0.000174 | 7.4 |
| QS-CM-SD-6 | 1.42E−05 | 1.18 | 0.000178 | 6.9 |
| QS-CM-SD-7 | 1.42E−03 | 1.25 | 0.000179 | 7.0 |
| QS-CM-SD-8 | 1.42E−03 | 1.41 | 0.000183 | 7.8 |
| QS-CM-SD-9 | 1.42E−03 | 1.32 | 0.000184 | 7.2 |
| QS-HP-S-1 | 3.85E−06 | 0.31 | 0.000144 | 2.6 |
| QS-HP-S-2 | 3.85E−06 | 0.32 | 0.000119 | 2.7 |
| QS-HP-S-3 | 3.85E−06 | 0.32 | 0.000129 | 2.5 |
| QS-HP-S-4 | 3.85E−05 | 0.34 | 0.000172 | 2.5 |
| QS-HP-S-5 | 3.85E−05 | 0.36 | 0.000158 | 2.7 |
| QS-HP-S-6 | 3.85E−05 | 0.36 | 0.000127 | 2.9 |
| QS-HP-S-7 | 3.85E−03 | 0.43 | 0.000196 | 2.8 |
| QS-HP-S-8 | 3.85E−03 | 0.46 | 0.000185 | 2.8 |
| QS-HP-S-9 | 3.85E−03 | 0.45 | 0.000147 | 2.9 |
| QS-HP-SD-1 | 3.85E−06 | 0.33 | 0.000108 | 3.1 |
| QS-HP-SD-2 | 3.85E−06 | 0.36 | 0.000147 | 2.7 |
| QS-HP-SD-3 | 3.85E−06 | 0.35 | 0.000138 | 2.6 |
| QS-HP-SD-4 | 3.85E−05 | 0.38 | 0.000147 | 2.7 |
| QS-HP-SD-5 | 3.85E−05 | 0.36 | 0.000146 | 2.7 |
| QS-HP-SD-6 | 3.85E−05 | 0.38 | 0.000129 | 3.0 |
| QS-HP-SD-7 | 3.85E−03 | 0.41 | 0.000163 | 2.9 |
| QS-HP-SD-8 | 3.85E−03 | 0.44 | 0.000192 | 2.8 |
| QS-HP-SD-9 | 3.85E−03 | 0.43 | 0.000147 | 3.1 |

*QS* quasi-static state, *CM* common mortar, *HP* high-porosity mortar, *S and SD* are fully saturated and saturated-then-dried specimens

## Appendix B: Dynamic test results

See Tables 3 and 4

**Table 3** Summary of dynamic test results for common mortar

| Specimen No | $\dot{\varepsilon}$ ($s^{-1}$) | Loading rate (GPa/s) | $f_t$ (MPa) | Strain (mm/mm) | $E$ (GPa) | $DIF_{ft}$ | $DIF_E$ | Enhancing Specific value |
|---|---|---|---|---|---|---|---|---|
| DB-CM-S-01 | 0.94 | 6.31 | 1.32 | 0.000239 | 6.9 | 1.21 | 1.28 | 1.16 |
| DB-CM-S-02 | 1.15 | 7.74 | 1.38 | 0.000254 | 6.9 | 1.27 | 1.37 | 1.24 |
| DB-CM-S-03 | 1.26 | 8.50 | 1.48 | 0.000249 | 7.4 | 1.36 | 1.34 | 1.17 |
| DB-CM-S-04 | 1.53 | 10.31 | 1.53 | 0.000253 | 7.0 | 1.40 | 1.36 | 1.10 |
| DB-CM-S-05 | 1.54 | 10.37 | 1.60 | 0.000253 | 7.4 | 1.46 | 1.36 | 1.26 |
| DB-CM-S-06 | 1.65 | 11.13 | 1.61 | 0.000262 | 7.5 | 1.47 | 1.41 | 1.22 |
| DB-CM-S-07 | 1.67 | 11.24 | 1.72 | 0.000310 | 7.5 | 1.57 | 1.67 | 1.28 |
| DB-CM-S-08 | 1.91 | 12.86 | 1.69 | 0.000309 | 8.3 | 1.55 | 1.66 | 1.14 |
| DB-CM-S-09 | 1.91 | 12.87 | 1.82 | 0.000373 | 8.6 | 1.66 | 2.01 | 1.29 |
| DB-CM-S-10 | 2.04 | 13.75 | 1.85 | 0.000310 | 8.5 | 1.69 | 1.67 | 1.18 |
| DB-CM-S-11 | 2.17 | 14.61 | 1.85 | 0.000328 | 8.4 | 1.69 | 1.77 | 1.32 |
| DB-CM-S-12 | 2.24 | 15.07 | 1.91 | 0.000383 | 8.6 | 1.74 | 2.06 | 1.37 |
| DB-CM-S-13 | 2.39 | 16.11 | 1.98 | 0.000346 | 8.3 | 1.82 | 1.86 | 1.23 |
| DB-CM-S-14 | 2.50 | 16.83 | 2.19 | 0.000328 | 8.8 | 2.00 | 1.76 | 1.43 |
| DB-CM-S-15 | 2.66 | 17.94 | 2.25 | 0.000373 | 8.8 | 2.06 | 2.01 | 1.32 |
| DB-CM-SD-1 | 1.27 | 8.92 | 1.45 | 0.000246 | 7.0 | 1.22 | 1.46 | |
| DB-CM-SD-2 | 1.34 | 9.41 | 1.41 | 0.000257 | 7.4 | 1.19 | 1.52 | |
| DB-CM-SD-3 | 1.43 | 10.09 | 1.45 | 0.000269 | 7.5 | 1.22 | 1.60 | |
| DB-CM-SD-4 | 1.57 | 11.04 | 1.57 | 0.000241 | 7.7 | 1.33 | 1.43 | |
| DB-CM-SD-5 | 1.81 | 12.76 | 1.58 | 0.000301 | 7.6 | 1.33 | 1.79 | |
| DB-CM-SD-6 | 1.86 | 13.12 | 1.66 | 0.000258 | 8.1 | 1.40 | 1.53 | |
| DB-CM-SD-7 | 1.91 | 13.42 | 1.63 | 0.000268 | 8.0 | 1.38 | 1.59 | |
| DB-CM-SD-8 | 2.09 | 14.71 | 1.60 | 0.000251 | 8.2 | 1.35 | 1.49 | |
| DB-CM-SD-9 | 2.20 | 15.49 | 1.76 | 0.000294 | 9.1 | 1.48 | 1.75 | |
| DB-CM-SD-10 | 2.33 | 16.36 | 1.82 | 0.000282 | 8.9 | 1.54 | 1.68 | |
| DB-CM-SD-11 | 2.55 | 17.97 | 1.88 | 0.000243 | 8.6 | 1.59 | 1.44 | |
| DB-CM-SD-12 | 2.60 | 18.28 | 1.83 | 0.000311 | 8.5 | 1.54 | 1.85 | |
| DB-CM-SD-13 | 2.71 | 19.06 | 1.96 | 0.000295 | 8.6 | 1.65 | 1.75 | |
| DB-CM-SD-14 | 2.93 | 20.59 | 2.11 | 0.000257 | 9.4 | 1.78 | 1.53 | |
| DB-CM-SD-15 | 2.94 | 20.71 | 2.20 | 0.000268 | 10.5 | 1.85 | 1.59 | |

*DB* Dynamic-Brazilian disc tests

**Table 4** Summary of dynamic test results for high-porosity mortar

| Specimen No | $\dot{\varepsilon}$ ($s^{-1}$) | Loading rate (GPa/s) | $f_t$ (MPa) | Strain (mm/mm) | $E$ (GPa) | $DIF_{ft}$ | $DIF_E$ | Enhancing Specific value |
|---|---|---|---|---|---|---|---|---|
| DB-HP-S-01 | 1.50 | 3.89 | 0.53 | 0.000213 | 3.5 | 1.68 | 1.35 | 1.16 |
| DB-HP-S-02 | 1.70 | 4.42 | 0.60 | 0.000196 | 4.0 | 1.88 | 1.56 | 1.24 |
| DB-HP-S-03 | 1.84 | 4.78 | 0.58 | 0.000230 | 3.9 | 1.83 | 1.52 | 1.17 |
| DB-HP-S-04 | 1.94 | 5.06 | 0.56 | 0.000272 | 3.9 | 1.75 | 1.52 | 1.10 |
| DB-HP-S-05 | 1.99 | 5.17 | 0.65 | 0.000242 | 4.3 | 2.03 | 1.64 | 1.26 |
| DB-HP-S-06 | 2.12 | 5.52 | 0.67 | 0.000227 | 4.1 | 2.11 | 1.58 | 1.22 |
| DB-HP-S-07 | 2.34 | 6.08 | 0.67 | 0.000207 | 4.3 | 2.11 | 1.65 | 1.28 |
| DB-HP-S-08 | 2.66 | 6.92 | 0.66 | 0.000322 | 4.6 | 2.09 | 1.75 | 1.14 |
| DB-HP-S-09 | 2.73 | 7.10 | 0.76 | 0.000279 | 4.2 | 2.40 | 1.61 | 1.29 |
| DB-HP-S-10 | 3.15 | 8.19 | 0.75 | 0.000230 | 4.4 | 2.35 | 1.70 | 1.18 |
| DB-HP-S-11 | 3.30 | 8.58 | 0.86 | 0.000226 | 4.6 | 2.70 | 1.76 | 1.32 |
| DB-HP-S-12 | 3.64 | 9.47 | 0.94 | 0.000289 | 4.5 | 2.97 | 1.73 | 1.37 |
| DB-HP-S-13 | 4.11 | 10.69 | 0.91 | 0.000319 | 5.2 | 2.85 | 1.99 | 1.23 |
| DB-HP-S-14 | 4.73 | 12.29 | 1.14 | 0.000401 | 5.7 | 3.61 | 2.20 | 1.43 |
| DB-HP-S-15 | 4.76 | 12.37 | 1.07 | 0.000371 | 5.5 | 3.36 | 2.11 | 1.32 |
| DB-HP-SD-01 | 1.31 | 3.66 | 0.45 | 0.000240 | 3.1 | 1.29 | 1.09 | |
| DB-HP-SD-02 | 1.60 | 4.47 | 0.46 | 0.000198 | 3.2 | 1.34 | 1.15 | |
| DB-HP-SD-03 | 1.67 | 4.66 | 0.51 | 0.000183 | 3.8 | 1.48 | 1.36 | |
| DB-HP-SD-04 | 2.38 | 6.66 | 0.55 | 0.000187 | 3.6 | 1.58 | 1.30 | |
| DB-HP-SD-05 | 2.77 | 7.76 | 0.57 | 0.000224 | 4.5 | 1.64 | 1.61 | |
| DB-HP-SD-06 | 3.03 | 8.47 | 0.61 | 0.000184 | 4.5 | 1.77 | 1.62 | |
| DB-HP-SD-07 | 3.45 | 9.66 | 0.66 | 0.000242 | 5.0 | 1.89 | 1.79 | |
| DB-HP-SD-08 | 4.05 | 11.32 | 0.69 | 0.000211 | 5.2 | 1.97 | 1.86 | |
| DB-HP-SD-09 | 4.14 | 11.58 | 0.72 | 0.000226 | 5.2 | 2.06 | 1.86 | |
| DB-HP-SD-10 | 4.16 | 11.63 | 0.74 | 0.000322 | 5.3 | 2.13 | 1.89 | |
| DB-HP-SD-11 | 4.33 | 12.12 | 0.78 | 0.000186 | 5.6 | 2.24 | 2.00 | |
| DB-HP-SD-12 | 4.42 | 12.37 | 0.78 | 0.000241 | 5.3 | 2.25 | 1.91 | |
| DB-HP-SD-13 | 4.88 | 13.66 | 0.81 | 0.000281 | 5.7 | 2.33 | 2.04 | |
| DB-HP-SD-14 | 5.12 | 14.31 | 0.85 | 0.000221 | 5.6 | 2.46 | 1.99 | |
| DB-HP-SD-15 | 5.29 | 14.81 | 0.90 | 0.000239 | 5.7 | 2.59 | 2.05 | |

## References


1. Xia K, Yao W (2015) Dynamic rock tests using split Hopkinson (Kolsky) bar system—a review. J Rock Mech Geotech Eng 7(1):27–59
2. Zhang X et al (2012) Laboratory test on dynamic material properties of annealed float glass. Int J Prot Struct 3(4):407–430
3. Joo Kim D et al (2010) Numerical simulation of the split Hopkinson pressure bar test technique for concrete under compression. Int J Impact Eng 37(2):141–149
4. Hao Y, Hao H, Zhang X (2012) Numerical analysis of concrete material properties at high strain rate under direct tension. Int J Impact Eng 39(1):51–62
5. Zhang X et al (2016) Static and dynamic material properties of CFRP/epoxy laminates. Constr Build Mater 114(Supplement C):638–649
6. Zhang X et al (2015) The mechanical properties of Polyvinyl Butyral (PVB) at high strain rates. Constr Build Mater 93(Supplement C):404–415
7. Rossi P et al (1992) The dynamic behaviour of concrete: influence of free water. Mater Struct 25:509–514
8. Yan D, Lin G (2006) Dynamic properties of concrete in direct tension. Cem Concr Res 36(7):1371–1378
9. Liu BD et al (2014) Effect of moisture content on static compressive elasticity modulus of concrete. Constr Build Mater 69:133–142

10. Cadoni E et al (2001) Strain-rate effect on the tensile behaviour of concrete at different relative humidity levels. Mater Struct 34:21–26
11. Huang X et al (2020) Equation of state for saturated concrete: a mesoscopic study. Int J Impact Eng 144:103669
12. Huang X et al (2020) The influence of free water content on ballistic performances of concrete targets. Int J Impact Eng 139:103530
13. Rossi P (1991) Influence of cracking in the presence of free water on the mechanical behaviour of concrete. Mag Concr Res 43(154):53–57
14. Sercombe J, Ulm F-J, Toutlemonde F (1998) Visous hardening plasticity for concrete in high-rate dynamic. J Eng Mech 124(9):1050–1057
15. Jin L, Du X, Ma G (2012) Macroscopic effective moduli and tensile strength of saturated concrete. Cem Concr Res 42(12):1590–1600
16. Wang H, Jin W, Li Q (2009) Saturation effect on dynamic tensile and compressive strength of concrete. Adv Struct Eng 12(2):279–286
17. Rossi P et al (1994) Effect of loading rate on the strength of concete subjected to uniaxial tension. Mater Struct 27:260–264
18. Wu S, Chen X, Zhou J (2012) Influence of strain rate and water content on mechanical behavior of dam concrete. Constr Build Mater 36:448–457
19. Zhang X et al (2012) Laboratory test on dynamic material properties of annealed float glass. Int J Prot Struct 3(4):407–430
20. Zhang X, Hao H, Ma G (2015) Dynamic material model of annealed soda-lime glass. Int J Impact Eng 77:108–119
21. Petrov YV et al (2017) Dynamic failure of dry and fully saturated limestone samples based on incubation time concept. J Rock Mech Geotech Eng 9(1):125–134
22. Huang S et al (2010) An experimental study of the rate dependence of tensile strength softening of Longyou sandstone. Rock Mech Rock Eng 43(6):677–683
23. Zhou Z et al (2019) Water saturation effects on dynamic fracture behavior of sandstone. Int J Rock Mech Min Sci 114:46–61
24. Wu L et al (2022) Peridynamic modeling for impact failure of wet concrete considering the influence of saturation. Int J Damage Mech 31(9):1448–1474
25. Colak A et al (2012) Surface adhesion and its dependence on surface roughness and humidity measured with a flat tip. Appl Surf Sci 258(18):6938–6942
26. Fuji M et al (1999) Effect of wettability on adhesion force between silica particles evaluated by atomic force microscopy measurement as a function of relative humidity. Langmuir 15(13):4584–4589
27. Jones R et al (2003) Inter-particle forces in cohesive powders studied by AFM: effects of relative humidity, particle size and wall adhesion. Powder Technol 132(2–3):196–210
28. Jones R et al (2002) Adhesion forces between glass and silicon surfaces in air studied by AFM: effects of relative humidity, particle size, roughness, and surface treatment. Langmuir 18(21):8045–8055
29. Gu H et al (2019) Dynamic fracture behaviour and evolution mechanism of soft coal with different porosities and water contents. Theor Appl Fract Mech 103, 102265
30. Zhou Z-L et al (2016) Influence of water content on mechanical properties of rock in both saturation and drying processes. Rock Mech Rock Eng 49(8):3009–3025
31. Cui Y et al (2017) Influential mechanism of pore water pressure on the compressive strength of concrete. In: 2nd International Conference on Architectural Engineering and New Materials
32. Accary A, Daudeville L, Malecot Y (2018) Investigation of the interstitial pore pressure of saturated concrete under high confinement. Proceedings 2(8):524. https://doi.org/10.3390/ICEM18-05397
33. Ge P et al (2021) Study on calculation model for compressive strength of water saturated recycled aggregate concrete. KSCE J Civ Eng 26(1):273–285
34. Sun X et al (2022) Effect of free water on fatigue performance of concrete subjected to compressive cyclic load. Constr Build Mater 318, 125995.
35. Beyene M, Meininger R (2022) A case study of distress mechanism(s) in a concrete structure foundation in the saturated zone and above the saturated zone. J Microsc 286(2):114–119
36. Hao X et al (2022) Comparative study of the effects of different nanomaterials on the failure process of saturated concrete in an underground reservoir of a coal mine. Energy Explor Exploit 40(6):1788–1805
37. Hu JY et al (2022) A review on corrosion detection and protection of existing reinforced concrete (RC) structures. Constr Build Mater 325, 126718.
38. Song X et al (2022) Cement-based repair materials and the interface with concrete substrates: characterization, evaluation and improvement. Polymers (Basel) 14(7), 1485. https://doi.org/10.3390/polym14071485
39. Fathy A, Zhu H, Kohail M (2022) Factors affecting the fresh-to-hardened concrete repair system. Constr Build Mater 320, 126279
40. Li et al., 2020, Post-blast performance and residual capacity of CFDST columns subjected to contact explosions. Journal of Constructional Steel Research, Vol. 167, 105960
41. Wang J et al (2023) Micro-nano scale pore structure and fractal dimension of ultra-high performance cementitious composites modified with nanofillers. Cement Concrete Compos 141, 105129
42. Uğur M, et al (2023) Comparison of effectiveness of blending and impregnation applications of dispersed nanoparticles on performance of cementitious composites. Constr Build Mater 392, 132009
43. Li L, et al (2022) Modifying fatigue performance of reactive powder concrete through adding pozzolanic nanofillers. Int J Fatigue 156, 106681
44. Singh Bhadauria S, Singh A (2022) Investigating mechanical characteristics of geopolymer concrete under the influence of Nano-fillers. Mater Today Proc 62:5159–5163
45. Luo Y, Brouwers HJH, Yu Q (2023) Understanding the gel compatibility and thermal behavior of alkali activated Class F fly ash/ladle slag: the underlying role of Ca availability. Cement Concrete Res 170, 107198
46. Teng L, et al (2023) Effect of competitive adsorption between specialty admixtures and superplasticizer on structural build-up and hardened property of mortar phase of ultra-high-performance concrete. Cement Concrete Compos 141, 105130

47. ASTM-International (2008) ASTM D-08. In: Standard test method for splitting tensile strength of intact rock core specimens. West Conshohocken, USA
48. Davies E, Hunter S (1963) The dynamic compression testing of solids by the method of the split Hopkinson pressure bar. J Mech Phys Solids 11(3):155–179
49. Davies R (1948) A critical study of the Hopkinson pressure bar. Philos Trans R Soc Lond Ser A Math Phys Sci 240(821):375–457
50. Hashiba K, Fukui K (2015) Effect of water on the deformation and failure of rock in uniaxial tension. Rock Mech Rock Eng 48(5):1751–1761
51. Martin BE et al (2009) Moisture effects on the high strain-rate behavior of sand. Mech Mater 41(6):786–798
52. Dudko OK et al (2003) Beyond the conventional description of dynamic force spectroscopy of adhesion bonds. Proc Natl Acad Sci 100(20):11378–11381
53. Xu Q et al (2014) Dynamic adhesion forces between microparticles and substrates in water. Langmuir 30(37):11103–11109